ACS APPLIED MATERIALS & INTERFACES

Article

Electrochemical Stimuli Driven Facile Metal Free Hydrogen Evolution from Pyrene-Porphyrin Based Crystalline Covalent Organic Framework.

Subhajit Bhunia, Sabuj Kanti Das, Rajkumar Jana, Sebastian C. Peter, Santanu Bhattacharya, Matthew Addicoat, Asim Bhaumik, and Anirban Pradhan

ACS Appl. Mater. Interfaces, **Just Accepted Manuscript** • DOI: 10.1021/acsami.7b06968 • Publication Date (Web): 26 Jun 2017

Just Accepted

ACS Publications

ACS Applied Materials & Interfaces is published by the American Chemical Society. 1155 Sixteenth Street N.W., Washington, DC 20036

Electrochemical Stimuli Driven Facile Metal Free Hydrogen Evolution from Pyrene-Porphyrin Based Crystalline Covalent Organic Framework.

Subhajit Bhunia,[†,‖] *Sabuj Kanti Das,*[‡,‖] *Rajkumar Jana,*[§] *Sebastian C Peter,*[§] *Santanu Bhattacharya,*[*,†] *Matthew Addicoat,*[*,¥] *Asim Bhaumik,*[*,‡] *and Anirban Pradhan*[*,†]

[†]Director's Research Unit, Indian Association for the Cultivation of Science, Jadavpur, Kolkata-700032, India.

[‡]Department of Material Science, Indian Association for the Cultivation of Science, Jadavpur, Kolkata- 700032, India.

[§]New Chemistry Unit, Jawaharlal Nehru Centre for Advanced Scientific Research, Jakkur, Bangalore- 560064, India

[¥]School of Science and Technology, Nottingham Trent University, Nottingham, NG11 8NS, UK.

ABSTRACT:

A [2+2] Schiff base type condensation between 5, 10, 15, 20-tetrakis(4-aminophenyl)porphyrin (TAP) and 1,3,6,8-tetrakis (4-formylphenyl) pyrene (TFFPy) under solvothermal condition yields a crystalline, quasi-two dimensional covalent organic framework (SB-PORPy-COF). The porphyrin and pyrene units are alternatively occupied in the vertex of 3D triclinic crystal having permanent micro-porosity with moderately high surface area (~869 m^2g^{-1}) and promising chemical stability. The AA stacking of the monolayers give a pyrene bridged conducting channel. SB-PORPy-COF has been exploited for metal free hydrogen production to understand the electrochemical behavior using the imine based docking site in acidic media. SB-PORPy-COF has shown the onset potential of 50 mV and the Tafel slope of 116 mV dec^{-1}. We expect that the addendum of the imine based COF would not only enrich the structural variety but also help to understand the electrochemical behavior of these class of materials.

KEYWORDS: Covalent organic framework, Porosity, Hydrogen evolution reaction, Electrochemical, Metal free, Porphyrin based.

1. INDRODUCTION

Covalent organic frameworks (COFs)[1-6] constructed from organic building blocks via covalent bonds are a unique kind of crystalline porous material with structural periodicity and inherent porosity of uniform topology. Besides them, recently some unique strategy has been developed to obtain morphologically tunable crystalline highly porous carbon materials by controlled thermal annealing of crystalline MOFs.[7-9] Due to the atomically precise pore apertures, resulting from strong and rigid covalent linkages between light elements (H, B, C, N and O) through the thermodynamically controlled reversible bond formation, COFs often show excellent and unique properties such as gas storage and separation,[10-14] molecular catalysis,[15-19] drug delivery [20-22] etc.

The two-dimensional COFs are more promising than the three-dimensional COFs because of two factors. The first factor is due to the inherent stacking between the two adjacent layers (π-π interaction). Because of the stacking phenomena, 2D COFs expedite the charge carrier mobility[22-24] through the multi-stacked columnar channel which results in promising optoelectronic phenomena, conductivity[25-28] and electroactivity[29-32] etc. The connectivity of the selected organic building blocks plays an important role on COFs' geometry[33, 34] which may lead to the formation of two dimensional (2D) or three dimensional (3D) crystalline networks having different pore apertures. Selecting and comprising some electro-active molecular unit such as porphyrin[35, 36], phthalocyanine, pyrene,[37] tetrathiafulvalene and thiophene[38, 39] derivatives, the stacking pattern may be tuned to different extent such as AA (eclipsed), AB (staggered), serrated and inclined arrangements which results in the different extent of electronic coupling between two layers. The second factor is the degree of lateral conjugation from π orbitals present throughout the individual 2D layer. The molecular assembly of alternating donor acceptor moiety boosts the charge carrier mobility over the single layer. Electrochemical hydrogen production[40, 41] from water holds an exceptional promise towards sustainable source of carbon free high purity energy at low cost price. The development of productive electrocatalyst mainly consists of two factors, (1) the reaction kinetics of hydrogen production and (2) the overpotential value. Noble metal containing systems hold maximum hydrogen evolution reaction (HER) properties with low overpotential (η) than any other metal based system.[42, 43] In the past decades many attempts have been made to develop noble metal free system containing electrochemically responsive transition metals based Co, Fe, Ni, Mo-complexes. But often metal ions leaches away from making the electrocatalytic system toxic. The new challenge requires the invention of metal free electro-catalyst to overcome the environmental hazard and facilitate the greener way of

production of clean and high purity energy. The π-electronic conjugation, low band gap and active side-groups etc. make an organic system electrochemically responsive. So a proper tuning of these properties for developing a metal free electrocatalyst by varying molecular architecture and assembly makes the process challenging and demanding. To the best of our knowledge, there is no report in literature which describes metal free hydrogen evolution from a covalent organic framework.

Herein we have developed a 2D COF named SB-PORPy by the selection of two monomer units with specific geometry under a homogeneous solution phase Schiff base condensation reaction. The [2+2] condensation of D_{2h} and D_{4h} (**Figure 1**) type building blocks is geometrically and topologically strained but the as synthesized material would be obtained in a crystalline form with uniform pore size which is confirmed from the PXRD pattern. For the first time we have focused on the electrochemical response of this pyrene-porphyrin comprised conjugated imine based covalent organic framework (SB-PORPy) in order to understand the charge carrier mobility of the metal free system having extensive π conjugation, pyrene core stimulated π-π stacking and durability, coming from reticular assembly.

2. EXPERIMENTAL SECTION

2.1. Materials

All reagents were supplied from commercial source and used without further purification. 5,10,15,20-Tetrakis(4-aminophenyl) porphyrin (TAP) was synthesized by previously reported procedure[44] which is described in supporting information (**ESI Section S1**). 1,3,6,8-tetrakis(4-formylphenyl) pyrene (TFFPy) was synthesized via new synthetic route for better yield. 1,3,6,8-tetrakis(4,4,5,5-tetramethyl-1,3,2-dioxaborolan-2-yl)pyrene (Py-$bpin_4$) was synthesized

following the previously reported procedure[45].Tetrakis (triphenylphosphine) palladium (0), [1,1′-Bis(diphenylphosphino)ferrocene]dichloropalladium(II) was received from sigma Aldrich. 4-fromyl phenyl boronic acid, Dimethyl acetamide, o-dichlorobenzene etc. were purchased from Spectrochem, India. Other solvents, acid, bases were supplied from local commercial source.

2.2. Instrumentation.

^{1}H and ^{13}C NMR were carried out using Bruker DPX-300 NMR spectrometer. Carbon, hydrogen and nitrogen contents of SB-PORPy-COF by Perkin Elmer 2400 Series II CHN analyzer. X-Ray powder diffraction patterns of the samples were obtained with a X'Pert PRO of PANalytical diffractometer using Cu Kα (= 0.15406 nm) radiation. Volumetric Nitrogen adsorption/desorption analysis, Brunauer-Emmett-Teller (BET) specific surface area, pore volume and micropore size etc were carried out at 77 K using Autosorb 1 (quantachrome,USA). Prior to adsorption measurement the samples were outgassed in vacuum at 150 ^{0}C for 10 h. NLDFT pore-size distribution was obtained from the adsorption/desorption isotherms by using the carbon/slit-cylindrical pore model. The ^{13}C cross-polarization magic angle spinning (CP-MAS) NMR spectrum was obtained from 500MHz Bruker-Avance II spectrometer at a mass frequency of 8 kHz. Thermogravimetry analysis (TGA) and differential thermal analyses (DTA) of the samples are carried out in a TGA Instruments thermal analyzer TA-SDT Q-600. A Hitachi S-5200 field-emission scanning electron microscope was used for the determination of the morphology of the particles. Transmission electron microscopy (TEM) images were obtained by a JEOL JEM 2010 transmission electron microscope operating at 100 kV. The samples were prepared by dropping a colloidal solution onto the carbon-coated copper grids followed by drying under high vacuum. The ^{1}H and ^{13}C NMR spectra were obtained from Bruker AVANCE III-400 MHz spectrometer. ^{1}H NMR spectra were collected at 400 MHz with chemical shift

referenced to the residual peak in $CDCl_3$ (δ: H 7.26ppm. Multiplicities are written as s (singlet), d (doublet), t (triplet), m (multiplet) and br (broad).

All the electrochemical measurements were performed on a CHI 760E electrochemical work-station with three electrode channels at room temperature. Three electrode set-up consists of a glassy carbon (GC) as working electrode, platinum wire as counter and saturated calomel electrode (SCE) as reference electrodes. The potentials measured were then corrected to the reversible hydrogen electrode (RHE) using the following equation ($E_{RHE} = E_{SCE}$+0.241 +0.059 pH) V at room temperature. The electrolyte solution was deaerated by purging nitrogen gas into the solution at least 30 min before each experiment. The scan rate used for all linear sweep voltammetry study is 1 mV s^{-1}. The stability of the catalyst was determined by cyclic voltammetry (CV) carried out between 0.2V and -0.5V (vs. RHE) at a scan rate of 100 mVs^{-1} for 500 cycles. AC data obtained at -0.15V vs RHE with 5 mV ac amplitude in 0.5 (M) H_2SO_4. The frequency range used for the impedance measurement is 100 kHz to 10 mHz.

2.3. Synthesis of 1,3,6,8-tetrakis(4,4,5,5-tetramethyl-1,3,2-dioxaborolan-2-yl)pyrene (Py-bpin$_4$) (2)

A schlenk tube was charged with 1.5 g 1,3,6,8-tetrabromopyrene **1** (2.9 mmol), bis (pinacolato) diboron (4.4 g, 17.35 mmol), Pd(dppf)Cl_2 (0.175 g, 0.25 mmol) and potassium acetate (1.75 g, 17.85 mmol) in 15 ml anhydrous DMSO. The the mixture was backfilled with N_2 three times and heated the reaction mixture at 90°C for 48 h under stirring condition. The reaction mixture was cooled to room temperature and extracted with Dichloromethane (DCM). The crude product was isolated by solvent evaporation as a yellow solid. The crude was then purified by using flash column chromatography on silica gel (60-120 mesh) using dichloromethane/toluene as an eluent. The tetra borylated product **2** was isolated as grey solid (1.5 g, yield 76 %).

Mp: >300°C NMR: ^{1}H NMR (400 MHz, $CDCl_3$, ppm) 9.15 (s, 4H); 8.98 (s, 2H); 1.54 (s, 24H); 1.50 (s, 24H). ESI HRMS calcd (M+) 706.42115, found 706.419135. FTIR ν_{max} (neat/cm^{-1}): 2928, 1552, 1341, 1210, 1142, 1086, 1018, 961,858, 660.

2.3. Synthesis of 1,3,6,8-tetrakis(4-formylphenyl) pyrene (TFFPy) (3)

A mixture of 1,3,6,8-tetrakis(4,4,5,5-tetramethyl-1,3,2-dioxaborolan-2-yl)pyrene (1.4 g, 2 mmol) **2**, 4-bromo benzaldehyde (2.22 g, 12 mmol), palladium tetrakis(triphenylphosphine) (0.138 g, 0.12 mmol), and K_2CO_3 (1.6 g, 12 mmol) were placed in 20 ml dioxane/water mixture (16: 4). The mixture was backfilled with nitrogen three times and stirred under nitrogen for 3 days at 90 °C. The orange suspension reaction mixture was poured into ice water mixture. Then the yellow solid was filtered, and washed with dilute HCl. The product was repeatedly washed with diethyl ether (100 ml) and the product was dried in vacuum to give the 1,3,6,8-tetrakis(4-formylphenyl) pyrene (TFFPy) **3** as yellowish-orange solid (1.11 g, 90%).

Mp: >300°C. NMR: ^{1}H NMR (400 MHz, $CDCl_3$, ppm) 10.16 (s, 4H); 8.18 (s, 4H); 8.09 (d, J = 8.0 Hz, 8H); 8.04 (s, 2H); 7.86 (d, J = 8.0 Hz, 8H). ESI HRMS calcd (M+) 618.18103, found 618.18010. FTIR ν_{max} (neat/cm^{-1}): 3429, 2926, 2814, 2723, 1697, 1600, 1306, 1208, 831, 734.

2.4. Synthesis of SB-PORPy-COF

An dimethyl acetamide (DMAc)/ o-dichlorobenzene(o-DCB) (3.0/1.0 ml) mixture was added to the mixture of 5,10,15,20-Tetrakis(4-aminophenyl)porphyrin (0.1 mmol, 67 mg) and 1,3,6,8-tetrakis(4-formylphenyl) pyrene (0.1 mmol, 61 mg) using an acetic-acid catalyst (6 M, 0.5 ml) in a schlenk tube (50 ml) and sonicated for 1h . Then the tube was degassed via three freeze–pump–thaw cycles and flame sealed under vacuum and heated statically in oven at 120 °C for 7-8 days. The greenish-brown precipitate was collected via centrifugation, washed Several times

with THF to remove the trapped guest molecules. The powder was collected and dried at 120 °C under vacuum overnight to produce SB-PORPy-COF in an isolated yield of 76 %.

2.5. Catalyst Preparation:

Vulcan supported SB-PORPy-COF catalyst has been prepared by mechanical grinding with Vulcan in 1:1 weight ratio. The catalyst ink was prepared by dispersing 2 mg of the composite catalyst in 1 mL of mixed solvent solution (IPA: H_2O=1:1 v/v) and 20 µL of 0.5 wt% nafion binder. The nafion binder (5 wt%) was diluted to 0.5 wt% with isopropyl alcohol (IPA). From the prepared catalyst ink 10 µL was drop-casted on GC electrode (3 mm diameter) and dried overnight in air. Before depositing the catalyst, the GC electrode was polished with 0.05 µm alumina slurry, washed several times with distilled water.

3. RESULT AND DISCUSSION

In order to construct the crystalline SB-PORPy-COFs, we have selected tetra-armed 5,10,15,20-tetrakis (4-aminophenyl) porphyrin (TAP) (**ESI Section S1**) of D_{4h} symmetry and 1,3,6,8-tetrakis(4-formylphenyl) pyrene (TFFPy) (**compound 3**, **Figure 1A**) of D_{2h} symmetry as the starting building block. The acid catalyzed reversible solvothermal condensation between TAP and TFFPy (**Figure 1B**) in the solvent mixture of dimethylacetamide/ o-dichlorobenzene (3:1 by vol.) using 6(M) acetic acid under static heating at 120° C for 7 days produced SB-PORPy-COF as a greenish-brown powder which is insoluble in common organic solvents and even in strong inorganic acids and bases such as aqueous H_2SO_4 and NaOH. At first the COF synthesis had been optimized using different solvent system such as Mesitylene/Dioxane, dimethyl formamide, o-dichlorobenzene, Dioxane/n-Butanol and N,N dimethyl acetamide/o-dichlorobenzene

maintaining same molar ratio (1:1) of two monomers. Among those, the N,N dimethyl acetamide/o-dichlorobenzene solvent system was the best trial for obtaining the moderate surface area along with significant crystallinity. The extensive formation of imine linkage was detected by Fourier transform Infrared (FT-IR) and ^{13}C cross polarized (CP) solid state MAS NMR spectroscopic methods. It has been clearly seen that In FT-IR spectra (**Figure 2A**) the absorption band near 1601 cm^{-1} for the C=N bond stretching modes which states about the existence of imine functionality between the pyrene and porphyrin moiety. The structural integrity of the framework was confirmed by solid state CP-MAS NMR which displays the resonance signal around 159.7 ppm for the carbon of C=N bond (**Figure 2B**). The resonance peak around ~147.1 ppm can be assigned to the quaternary carbon of the organic framework. The peak around ~119.6 ppm is indicative of the methine carbon of the porphyrin macrocycle and at ~114.1 ppm for β-pyrrolic carbon. The biggest resonance peak around ~131.1 ppm is mainly due to the pyrenyl phenyl moiety of the covalent organic framework. The X-ray photo-electron spectroscopy (XPS) of SB-PORPy-COF had shown the broad peak centered around 399 eV which can be attributed to the N_{1S} and the peak around 284 eV which is for C_{1S}. The connectivity between the pyrene and porphyrin moiety via C=N bond formation, is directly reflected to deconvoluted N_{1s} spectra which is composed of three component peaks. The first, second and third component peaks are at 398, 399 and 400 eV respectively. The first peak (398 eV) is mainly due to presence pyrrolic nitrogen and pyrrolic -NH peak is present at the slight shifted higher binding energy region (400 eV) (**Figure 2C&D**). The 'N' atom associated with Schiff base bond (C=N) has shown the peak at 399 eV. The morphological analysis and porosity of SB-PORPy-COF has been investigated using scanning electron microscopy (SEM) (**figure 4D**) and high resolution transmission electron microscopy (HRTEM) respectively. Those revealed that SB-PORPy is composed of 80-

150 nm sized porous thin platelets with granular morphology respectively which has been shown in **Figure 2E & 2F** (HRTEM). The SB-PORPy COF has shown promising thermal stability upto 400 °C which was confirmed by the thermo gravimetric (TGA) analysis (ESI, **Fig S1**).

The possible crystal structure of the SB-PORPy-COF was obtained by the experimental XRD measurements along with theoretical structural simulations. The molecular assembly will be slightly topologically strained due to the geometries (D_{2h} and D_{4h}) of monomers. But the static heating of reaction mixture for long time (7 days) has made the SB-PORPy-COF crystalline. The strong XRD peaks at the position $2\theta = 4.9^{\circ}$ and $\sim 22^{\circ}$ which can be assigned to the (020), and (202) facets respectively. The hump centered at ~22° may be attributed to zigzag π-π stacking of 2D layers. The theoretical PXRD pattern of AA stacking model (black, **Figure 3B**) of SB-PORPy monolayers is in perfect agreement with the peak position and the intensity of the experimental obtained PXRD (blue, **Figure 3A**), whereas the AB stacking model (red, **Figure 3C**) is totally different. The theoretical quasi 2D eclipse structure (AA) and the staggered structure (AB) has shown in the **figure 3D & 3E**. The PXRD data obtained after Pawley refinement resulted (**Figure 3F**, blue curve) in a pattern that is exactly matching with the experimentally observed pattern (purple scattered asterisk, showing small difference **Figure 3F**, wine plot) giving the Pawley refinement factor (Rp) ~2.79%. A 3D triclinic unit cell (P_1 space group) having the parameters of a = 37.098 Å, b = 36.8016 Å, c = 8.06797 Å, $\alpha = 89.9333^{\circ}$, $\gamma = 89.9038^{\circ}$ and $\beta = 90.1005^{\circ}$ was derived from the theoretical optimization of SB-PORPy-COF (ESI **Section S4**). The absence of long range periodicity can be attributed to the fact that geometry of two building blocks (D_{2h} & D_{4h}) are slightly topologically overruled to give a strain free periodic structure. The permanent porosity of SB-PORPy-COF has been determined by measuring volumetric N_2 adsorption/desorption experiment at 77 K which exhibits type-I

isotherm which is the characteristic of intrinsic microporosity of COF SB-PORPy (**Figure 4A**). The Brunauer-Emmett-Teller surface area and the total pore volume are ~869 $m^2 g^{-1}$ and 0.51 $cm^3 g^{-1}$. The sample was activated at 160 $^{\circ}$C to remove the solvent molecule from the lattice for sorption analysis. The pore size distribution based on non-local density functional theory has shown an unimodal porosity having single peak at 1.7 nm (**Figure 4B**). The stability test of the SB-PORPy-COF material had been done by emerging the powder sample in various organic solvents such as THF, dioxane, toluene, DMF etc. for 7 days. There was no change of powder XRD pattern had been observed after solvent socking for 7 days. The material had shown the remarkable stability in aqueous, acidic (0.5 M) or alkaline (0.5 M) solution (**Figure 4C**). In this porous framework, the pyrene core is connected to the porphyrin moiety alternatively through the C=N linkage which creates the fluorescent channel in the 2D COF. The electronic absorption spectrum has shown a solid state broad absorption giving three maxima in the visible region. The maxima centered at 663 nm may be attributed to the α-Q band, 570 nm for β-Q band and 400 nm is for sorbet band of porphyrin unit present in the framework. The COF has the strong photoluminescence emission giving maxima at 688 nm (ESI, **Figure S2**).

3.1. Metal free electrochemical hydrogen evolution

Electrochemical activities of SB-PORPy-COF catalyst toward HER was investigated in 0.5 (M) H_2SO_4 solution. So, far hydrogen evolution catalyzed by any type of transition metal based complexes and materials in previous report, but electrocatalytic hydrogen evolution by any type of metal free COF has never been reported. A few cobalt complexes including cobalt porphyrin were testified to be an effective electrocatalyst for electrocatalytic HER[46-48]. However, very high overpotentials were required for such systems. In general, only COFs have been used to support

the porosity and large surface area for the electrocatalysts [49,50] An efficient electrocatalysts can also be developed through rational designing of COFs.[51] In the following study, SB-PORPy COF had shown to be an efficient metal free electrocatalyst with a remarkably low onset overpotential of ~50 mV which is the lowest reported overpotential ever for any types of COFs (**Figure 5A**) in acidic solution. From the linear sweep voltammetry curve, it is clear that the electro-catalytic activities of bare glassy carbon (GC) and Vulcan were negligibly small. HER as reflected by low current density and very high overpotential for pure Vulcan (red curve, **Figure 5A**) whereas Vulcan/COF/GC represents a much larger current density with extremely low overpotential for HER (black curve, **Figure 5A**). This was the indication of a pronounced electro-activity of the as synthesized SB-PORPy-COF. This result clearly indicates that principal contribution towards HER comes from as synthesized SB-PORPy-COF and confirms about it's electro-activity towards hydrogen evolution reaction. The conductive Vulcan carbon has only been used to enhance the conductivity of the system. The potential to achieve 1 mA/cm^2 was found to be -0.2V vs RHE which is better than any cobalt based COF systems. More interestingly, overpotential required for 5 mA cm^{-2} exchange current density is as low as 380 mV indicating extraordinary activity towards hydrogen evolution reaction in terms of COF based systems. HER mechanism can be well-reflected from the Tafel slope involving the following three steps occuring on the catalyst surface.

Step-1 Volmer: $H^+ + e^- \longrightarrow H_{ads}$

Step-2 Heyrovsky: $H_{ads} + H^+ + e^- \longrightarrow H_2$

Step-3 Tafel: $H_{ads} + H_{ads} \longrightarrow H_2$

Step 1 is the adsorption step and desorption step on porous surface of electrocatalyst. H_2 evolution can happen either through Step 2 (Heyrovsky) or Step 3 (Tafel). Therefore, total H_2

evolution reaction will happen either following Volmer-Heyrovsky or Volmer-Tafel mechanism. A Tafel slope value of 30 mV/dec will indicates rate determining step (r.d.s.) to be Tafel whereas 40 mV/dec and 120 mV/dec will respectively indicate Heyrovsky and Volmer will be the r.d.s.[52-55].The linear nature of the Tafel slope obtained from the polarization curve was ~116 mV.dec^{-1} indicating Volmer-Heyrovsky mechanism for the HER on the SB-PORPy COF surface and the Volmer step is the rate determining step (**Figure 5B**). The imine nitrogen sites present in the COF (-N=) are considered as free docking sites for HER. In acidic solution, imine nitrogen atoms are protonated making the moiety positively charged hyperporphyrinic structure whereas SO_4^{2-} maintains the electro-neutrality. On the other hand, H-H combination occurred with the help of other adjacent imine nitrogen sites facilitating the hydrogen evolution process from the surface **(Figure 6)**.

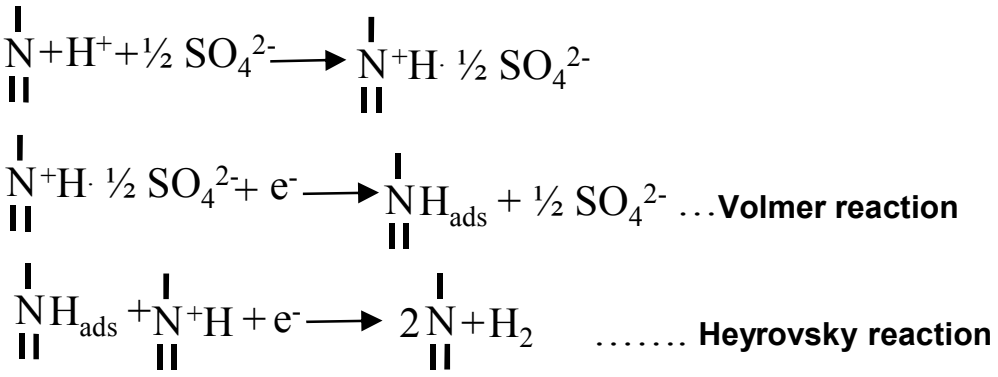

A general scheme can be considered from the electrochemical impedance spectroscopy which is a useful tool for studying the electrode kinetics in HER. **Figure 5C** represents Nyquist plot of SB-PORPy-COF catalyst in the frequency range 100 kHz to 10 MHz at -0.15V vs RHE in 0.5 M H_2SO_4 solution. As evident from **Figure 5C**, only one semicircle was observed with no prominent Warburg impedance indicating kinetically controlled electrochemical reaction on electrode surface due to rapid ionic transportation in the electrolyte. The diameter of the

semicircle can be attributed to the charge-transfer resistance (R_{ct}). A low value of R_{ct} corresponds to the fast reaction kinetics on the catalyst surface. The SB-PORPy-COF catalyst showed a very small value of R_{ct} (~145 Ω) (**Figure. 5C**). One of the concerns of the HER catalysts is stability, many catalysts lose their activity after a few cycles. To evaluate the durability of the SB-PORPy-COF catalyst, a potential cycling was conducted in the potential range 0.2V to -0.5V vs RHE at a scan rate of 100 mVs^{-1} for 500 cycles. As shown in **Figure 5D**, there is almost no loss of activity observed in terms of both onset potential and current density at different potentials, indicating good stability of the catalyst in acidic solution. The XPS had been done for N_{1s} to investigate the chemical state of nitrogen atoms (pyrrolic N and Schiff base N) which was remained intact after 500 cycles which accounts about the promising stability in 0.5 (M) H_2SO_4 **(ESI Figure S3)**. The Faradaic efficiency (FE) of SB-PORPy-COF was evaluated to be 90 % which accounts about the purity of catalyst towards electrochemical hydrogen evolution (ESI **Figure S4, section S3**). The FE value is quite comparable to the other established electrocatalysts[56].

CONCLUSION

In summary, we have designed an imine based conjugated pyrene, porphyrin comprised microporous quasi-2D covalent organic framework. The reversibility of imine bond formation leads to the formation of thermodynamically controlled crystalline framework in spite of the topological restriction from the view point of molecular geometry. A π electronic conjugation between pyrene and porphyrin creates a conducting channel (AA stacking). We have investigated the charge carrier mobility and metal free hydrogen evolution by imposing some short of electrochemical stimulation on SB-PORPy-COF. As far as we know, till date there is no COF based catalyst known that enables metal free hydrogen evolution. Such COFs are stable

even in strongly acidic/alkaline conditions. Furthermore such topologically strained crystalline imine based covalent organic frameworks will increase the structural diversity of these (COFs) classes of materials and find abundant scope of utility and applicability to understand the electrochemical aspects of COFs.

ASSOCIATED CONTENT

Supporting Information

The Supporting Information (ESI) is available free of charge on the ACS Publications website. Synthetic procedures, IR, melting point, ^{1}H NMR, DTA- TGA, UV-vis, Photo luminescence, N1s XPS for stability, Faradaic efficiency and theoretical simulations are available in ESI.

AUTHOR INFORMATION

Corresponding Author

*Prof. S. Bhattacharya, Email. director@iacs.res.in

*Dr. A. Pradhan, Email. msap5@iacs.res.in

*Prof. A. Bhaumik, Email. msab@iacs.res.in

*Dr. M. Addicoat, Email. matthew.addicoat@ntu.ac.uk

Author Contributions

‖ Both author contributed equally.

The manuscript was written through contributions of all authors. All authors have given approval to the final version of the manuscript.

Notes

The authors declare no competing financial interest.

ACKNOWLEDGMENT

SB, SKD thank CSIR and UGC respectively for funding. AP acknowledges DST for funding through INSPIRE program. Prof. SB acknowledges support received from DST (J. C. Bose fellowship) and that from DRU at IACS. AB thanks DST for instrumental supports through DST Unit on Nanoscience. SCP & RKJ thanks DST for financial support.

REFFERENCES

(1) Xu, H.; Gao, J.; Jiang, D. Stable, Crystalline, Porous, Covalent Organic Frameworks as a Platform for Chiral Organocatalysts. *Nat. Chem.* **2015**, *7*, 905-912.

(2) Dalapati , S.; Addicoat, M.; Jin, S.; Sakurai, T.; Gao , J.; Xu , H.; Irle, S.; Seki, S.; Jiang, D. Rational Design of Crystalline Supermicroporous Covalent Organic Frameworks with Triangular Topologies. *Nat. Commun*. **2015**, *6*, 7786 doi: 10.1038/ncomms8786.

(3) Liu, Y.; Ma, Y.; Zhao, Y.; Sun, X.; Gándara, F.; Furukawa, H.; Liu, Z.; Zhu, H.; Zhu, C.; Suenaga, K.; Oleynikov, P.; Alshammari, A. S.; Zhang, X.; Terasaki, O.; Yaghi, O. M. Weaving of Organic Threads into a Crystalline Covalent Organic Framework. *Science* **2016,** *351*, 365-369.

(4) Huang, N.; Ding, X.; Kim, J.; Ihee, H.; Jiang, D. A Photoresponsive Smart Covalent Organic Framework. *Angew. Chem. Int. Ed.* **2015**, *54*, 8704-8707.

(5) Kandambeth, S.; Biswal, B. P.; Chaudhari, H. D.; Rout, K. C.; H., S. K.; Mitra, S.; Karak, S.; Das, Mukherjee, A. R.; Kharul, U. K.; Banerjee, R. Selective Molecular Sieving in Self-standing Porous Covalent Organic Framework Membranes. *Adv. Mater.* **2017**, *29*,

1603945.

(6) Bojdys, M. J.; Jeromenok, J.; Thomas, A.; Antonietti, M. Rational Extension of the Family of Layered, Covalent, Triazine-Based Frameworks with Regular Porosity. *Adv. Mater.* **2010**, *22*, 2202-2205.

(7) Tang, J.; Yamauchi, Y. Carbon materials: MOF Morphologies in Control. *Nat. Chem.* **2016**, *8*, 638-639.

(8) Salunkhe, R. R.; Young, C.; Tang, J.; Takei, T.; Ide, Y.; Kobayashi, N.; Yamauchi, Y. A High-Performance Supercapacitor Cell Based on ZIF-8-Derived Nanoporous Carbon using an Organic Electrolyte. *Chem. Commun.* **2016**, *52*, 4764-4767.

(9) Salunkhe, R. R.; Kamachi, Y.; Torad, N. L.; Hwang, S. M.; Sun, Z. Q.; Dou, S. X.; Kim, J. H.; Yamauchi, Y. Fabrication of Symmetric Supercapacitors Based on MOF-Derived Nanoporous Carbons. *J. Mater. Chem. A* **2014**, *2*, 19848-19854.

(10) Rabbani, M. G.; Sekizkardes, A. K.; Kahveci, Z.; Reich, T. E.; Ding, R. E; El-Kaderi, H. M. A 2D Mesoporous Imine-Linked Covalent Organic Framework for High Pressure Gas Storage Applications. *Chem. Eur. J.* **2013**, *19*, 3324-3328.

(11) Shan, M.; Seoane, B.; Rozhko, E.; Dikhtiarenko, A.; Clet, G.; Kapteijn, F.; Gascon, J. Azine-Linked Covalent Organic Framework (COF)-Based Mixed-Matrix Membranes for CO_2/CH_4 Separation. *Chem. Eur. J.* **2016**, *22*, 14467-14470.

(12) Huang, N.; Chen, X.; Krishna, R.; Jiang, D. Two-Dimensional Covalent Organic Frameworks for Carbon Dioxide Capture through Channel-Wall Functionalization. *Angew. Chem. Int. Ed.* **2015**, 54, 2986-2990.

(13) Furukawa, F.; Yaghi, O. M. Storage of Hydrogen, Methane, and Carbon Dioxide in Highly Porous Covalent Organic Frameworks for Clean Energy Applications. *J. Am.*

Chem. Soc., **2009**, *131*, 8875-8883.

(14) Li, X. D.; Zang, H. P.; Wang, J. T.; Wang, J. F.; Zhang, H. Design of Tetraphenyl Silsesquioxane Based Covalent-Organic Frameworks as Hydrogen Storage Materials. *J. Mater. Chem. A* **2014**, *2*, 18554-18561.

(15) Shi, X.; Yao, Y.; Xu, Y.; Liu, K.; Zhu, G.; Chi, L.; Lu, G. Imparting Catalytic Activity to a Covalent Organic Framework Material by Nanoparticle Encapsulation. *ACS Appl. Mater. Interfaces* **2017**, *9*, 7481-7488.

(16) Shinde, D. B.; Kandambeth, S.; Pachfule, P.; Kumar, R. R.; Banerjee, R. Bifunctional Covalent Organic Frameworks with Two Dimensional Organocatalytic Micropores. *Chem. Commun.* **2015**, *51*, 310-313.

(17) Peng, Y.; Hu, Z.; Gao, Y.; Yuan, D.; Kang, Z.; Qian, Y.; Yan, N.; Zhao, D. Synthesis of a Sulfonated Two-Dimensional Covalent Organic Framework as an Efficient Solid Acid Catalyst for Biobased Chemical Conversion. *ChemSusChem.* **2015***, 8,* 3208-3212.

(18) Xu, H.; Chen, X.; Gao, J.; Lin, J.; Addicoat, M.; Irle, S.; Jiang, D. Catalytic Covalent Organic Frameworks via Pore Surface Engineering. *Chem. Commun.* **2014**, *50*, 1292-1294.

(19) Li, P. -Z.; Wang, X. -J.; Liu, J.; Lim, J. S.; Zou, R.; Zhao, Y. A Triazole-Containing Metal-Organic Framework as a Highly Effective and Substrate Size-Dependent Catalyst for CO_2 Conversion. *J. Am. Chem. Soc.* **2016**, *138*, 2142-2145.

(20) Fang, Q.; Wang, J.; Gu, S.; Kaspar, R, B.; Zhuang, Z.; Zheng, J.; Guo, H.; Qiu, S.; Yan, Y. 3D Porous Crystalline Polyimide Covalent Organic Frameworks for Drug Delivery. *J. Am. Chem. Soc.* **2015**, 137, 8352-8355.

(21) Bai, L.; Phua, S. Z. F.; Lim, W. Q.; Jana, A.; Luo, Z.; Tham, H. P.; Zhao, L.; Gao, Q.;

Zhao, Y. Nanoscale Covalent Organic Frameworks as Smart Carriers for Drug Delivery. *Chem. Commun.* **2016**, *52*, 4128-4131.

(22) Vyas, V. S.; Vishwakarma, M.; Moudrakovski, I.; Haase, F.; Savasci, G.; Ochsenfeld, C.; Spatz, J. P.; Lotsch, B. V. Exploiting Noncovalent Interactions in an Imine-Based Covalent Organic Framework for Quercetin Delivery. *Adv Mater.* **2016**, *28*, 8749-8754.

(23) Wan, S.; Gándara, F.; Asano, A.; Furukawa, H.; Saeki, A.; Dey, S. K.; Liao, L.; Ambrogio, M. W.; Botros, Y. Y.; Duan, X.; Seki, S.; Stoddart, J. F.; Yaghi, O. M. Covalent Organic Frameworks with High Charge Carrier Mobility. *Chem. Mater.* **2011**, *23*, 4094-4097.

(24) Ding, X.; Guo, J.; Feng, X.; Honsho, Y.; Guo, J.; Seki, S.; Maitarad, P.; Saeki, A.; Nagase, S.; Jiang, D. Synthesis of Metallophthalocyanine Covalent Organic Frameworks That Exhibit High Carrier Mobility and Photoconductivity. *Angew. Chem. Int. Ed.* **2011**, *50*, 1289-1293.

(25) He, T.; Pachfule, P.; Wu, H.; Xu, Q.; Chen, P. Hydrogen Carriers. *Nat. Rev. Mater.* **2016***, 1, 16059*.

(26) Yang, H.; Zhang, S.; Han, L.; Zhang, Z.; Xue, Z.; Gao, J.; Li, Y.; Huang, C.; Yi, Y.; Liu, H.; Li, Y. High Conductive Two-Dimensional Covalent Organic Framework for Lithium Storage with Large Capacity. *ACS Appl. Mater. Interfaces* **2016**, *8*, 5366-5375.

(27) Cai, S. L.; Zhang, Y. B.; Pun, A. B.; He, B.; Yang, J.; Toma, F. M.; Sharp, I. D.; Yaghi, O. M. Fan, J.; Zheng, S. R.; Zhang, W. G.; Liu, Y. Tunable Electrical Conductivity in Oriented Thin Films of Tetrathiafulvalene-Based Covalent Organic Framework. *Chem. Sci.* **2014**, *5*, 4693-4700.

(28) Nath, B.; Li, W.-H.; Huang, J. -H.; Wang, G. -E.; Fu, Z. -H.; Yao, M. -S.; Xu, G. A New

Azodioxy-linked Porphyrin-Based Semiconductive Covalent Organic Framework with I_2 Doping-Enhanced Photoconductivity. *CrystEngComm*. **2016**, *18*, 4259-4263.

(29) Smith, B. J.; Hwang, N.; Chavez, A. D.; Novotney J. L.; Dichtel, W. R. Growth Rates and Water Stability of 2D Boronate Ester Covalent Organic Frameworks. *Chem. Commun.* **2015**, *51*, 7532-7535.

(30) Medina, D. D.; Werner, V.; Auras, F.; Tautz, R.; Dogru, M.; Schuster, J.; Linke, S.; Döblinger, M.; Feldmann, J.; Knochel, P.; Bein, T. Oriented Thin Films of a Benzodithiophene Covalent Organic Framework. *ACS Nano* **2014**, *8*, 4042-4052.

(31) Wang, P.; Wu, Q.; Han, L.; Wang, S.; Fang, S.; Zhang, Z.; Sun, S. Synthesis of Conjugated Covalent Organic Frameworks/Graphene Composite for Supercapacitor Electrodes. *RSC Adv.* **2015**, *5*, 27290-27294.

(32) Patra, B. C.; Khilari, S.; Satyanarayana, L.; Pradhan, D.; Bhaumik, A. A New Benzimidazole Based Covalent Organic Polymer Having High Energy Storage Capacity. *Chem. Commun.* **2016**, *52*, 7592-7595.

(33) Huang, Y. B.; Pachfule, P.; Sun, J. K.; Xu, Q. From Covalent–Organic Frameworks to Hierarchically Porous B-doped Carbons: A Molten-Salt Approach. *J. Mater. Chem. A* **2016**, *4*, 4273-4279.

(34) Lin, G.; Ding, H.; Yuan, D.; Wang, B.; Wang C. A Pyrene-Based, Fluorescent Three-Dimensional Covalent Organic Framework. *J. Am. Chem. Soc.* **2016**, *138*, 3302-3305.

(35) Dalapati, S.; Jin, E.; Addicoat, M.; Heine, T.; Jiang, D. Highly Emissive Covalent Organic Frameworks. *J. Am. Chem. Soc.* **2016**, *138*, 5797-5800.

(36) Neti, V. S. P. K.; Wu, X.; Deng, S.; Echegoyen L. Synthesis of a Phthalocyanine and Porphyrin 2D Covalent Organic Framework. *CrystEngComm*. **2013**, *15*, 6892-6895.

(37) Lin, S.; Diercks, C. S.; Zhang, Y. B.; Kornienko, N.; Nichols, E. M.; Zhao, Y.; Paris, A. R.; Kim, D.; Yang, P.; Yaghi, O. M.; Chang, C. J. Covalent Organic Frameworks Comprising Cobalt Porphyrins for Catalytic CO_2 Reduction in Water. *Science* **2015**, *349*, 1208-1213.

(38) Dalapati, S.; Jin, S.; Gao, J.; Xu, Y.; Nagai, A.; Jiang, D. An Azine-Linked Covalent Organic Framework. *J. Am. Chem. Soc.* **2013**, *135*, 17310-17313.

(39) Bertrand, G. H. V.; Michaelis, V. K.; Ong, T. C.; Griffin, R. G.; Dincă, M. Thiophene-Based Covalent Organic Frameworks. *Proc. Natl. Acad. Sci. U.S.A.* **2013**, *110*, 4923-4928.

(40) Ascherl, L.; Sick, T.; Margraf, J. T.; Lapidus, S. H.; Calik, M.; Hettstedt, C.; Karaghiosoff, K.; Döblinger, M.; Clark, T.; Chapman, K. W.; Auras, F.; Bein, T. Molecular docking sites designed for the generation of highly crystalline covalent organic frameworks. *Nat. Chem.* **2016**, *8*, 310-316.

(41) Stegbauer, L.; Schwinghammer, K.; Lotsch, B. V. A hydrazone-based covalent organic framework for photocatalytic hydrogen production. *Chem. Sci.* **2014**, *5*, 2789-2793.

(42) Gao, G.; Jiao, Y.; Waclawik, E. R.; Du. A. Single Atom (Pd/Pt) Supported on Graphitic Carbon Nitride as an Efficient Photocatalyst for Visible-Light Reduction of Carbon Dioxide. *J. Am. Chem. Soc.* **2016**, *138*, 6292-6297.

(43) Kaeffer, N.; Morozan, A.; Fize, J.; Martinez, E.; Guetaz, L.; Artero, V. The Dark Side of Molecular Catalysis: Diimine-Dioxime Cobalt Complexes Are Not the Actual Hydrogen Evolution Electrocatalyst in Acidic Aqueous Solutions. *ACS Catal.* **2016**, *6*, 3727-3737.

(44) Xue, Z.; Lee, P. P. S.; Wang, Y.; Kwong, D. W. J. ; Li, J.; Xin, J. H.; Wong, W.-K.;

Cheuk, K. K.L. Further Insight into Aryl Nitration of Tetraphenylporphyrin. *Tetrahedron* **2011**, *67*, 6030-6035.

(45) Sprick, R. S.; Jiang, J.-X.; Bonillo, B.; Ren, S.; Ratvijitvech, T.; Guiglion, P.; Zwijnenburg, M. A.; D. J. Adams; Cooper, A. I. Tunable Organic Photocatalysts for Visible-Light-Driven Hydrogen Evolution. *J. Am. Chem. Soc.* **2015**, *137*, 3265-3270.

(46) Fan, Z.; Luo, Z.; Huang, X.; Li, B.; Chen, Y.; Wang, J.; Hu, Y.; Zhang, H. Synthesis of 4H/*fcc* Noble Multimetallic Nanoribbons for Electrocatalytic Hydrogen Evolution Reaction. *J. Am. Chem. Soc.* **2016**, *138*, 1414-1419.

(47) Kamire, R. J.; Majewski, M. B.; Hoffeditz, W. L.; Phelan, B. T.; Farha, O. K. ; Hupp , J. T.; Wasielewski, M. R. Photodriven Hydrogen Evolution by Molecular Catalysts using Al_2O_3-Protected Perylene-3,4-Dicarboximide on NiO Electrodes. *Chem. Sci.* **2017**, *8*, 541-549.

(48) Huang, D.; Lu, J.; Li, S.; Luo, Y.; Zhao, C.; Hu, B.; Wang, M.; Shen, Y. Fabrication of Cobalt Porphyrin. Electrochemically Reduced Graphene Oxide Hybrid Films for Electrocatalytic Hydrogen Evolution in Aqueous Solution. *Langmuir* **2014**, *30,* 6990-6998.

(49) Aiyappa, H. B.; Thote, J.; Shinde, D.B.; Banerjee, R.; Kurungot, S. Cobalt-Modified Covalent Organic Framework as a Robust Water Oxidation Electrocatalyst. *Chem. Mater.* **2016**, *28*, 4375-4379

(50) Ma, W.; Yu, P.; Ohsaka, T.; Mao, L. An Efficient Electrocatalyst for Oxygen Reduction Reaction Derived from a Co-porphyrin-based Covalent Organic Framework. *Electrochem. Commun.* **2015**, *52*, 53-57.

(51) Lin, C. -Y.; Zhang, L.; Zhao, Z.; Xia, Z. Design Principles for Covalent Organic

Frameworks as Efficient Electrocatalysts in Clean Energy Conversion and Green Oxidizer Production. *Adv. Mater*. **2017**, *29*, 1606635.

(52) Gruba, Z.; Hukovic, M. M.; Babic, R.; Nanocrystalline and Coarse Grained Polycrystalline Nickel Catalysts for the Hydrogen Evolution Reaction. *Int. J. Hydrogen Energy* **2013**, *38*, 4437-444.

(53) Huang, D.; Lu, J.; Li, S.; Luo, Y.; Zhao, C.; Hu, B.; Wang, M.; Shen, Y. Fabrication of Cobalt Porphyrin. Electrochemically Reduced Graphene Oxide Hybrid Films for Electrocatalytic Hydrogen Evolution in Aqueous Solution. *Langmuir* **2014**, *30*, 6990-6998.

(54) Lv, H.; Xi, Z.; Chen, Z.; Guo, S.; Yu, Y.; Zhu, W.; Li, Q.; Zhang, X.; Pan, M.; Lu, G.; Mu, S.; Sun, S. A New Core/Shell NiAu/Au Nanoparticle Catalyst with Pt-like Activity for Hydrogen Evolution Reaction. *J. Am. Chem. Soc.* **2015**, *137*, 5859-5862.

(55) Pentland, N.; Bockris, J. O. M.; Sheldon, E. Hydrogen Evolution Reaction on Copper, Gold, Molybdenum, Palladium, Rhodium, and Iron. *J. Electrochem. Soc.* **1957**, *104*, 182-194.

(56) Vrubel, H.; Hu, X. Molybdenum Boride and Carbide Catalyze Hydrogen Evolution in both Acidic and Basic Solutions. *Angew. Chem. Int. Ed.* **2012**, *124*, 12875-12878.

Figure. 1

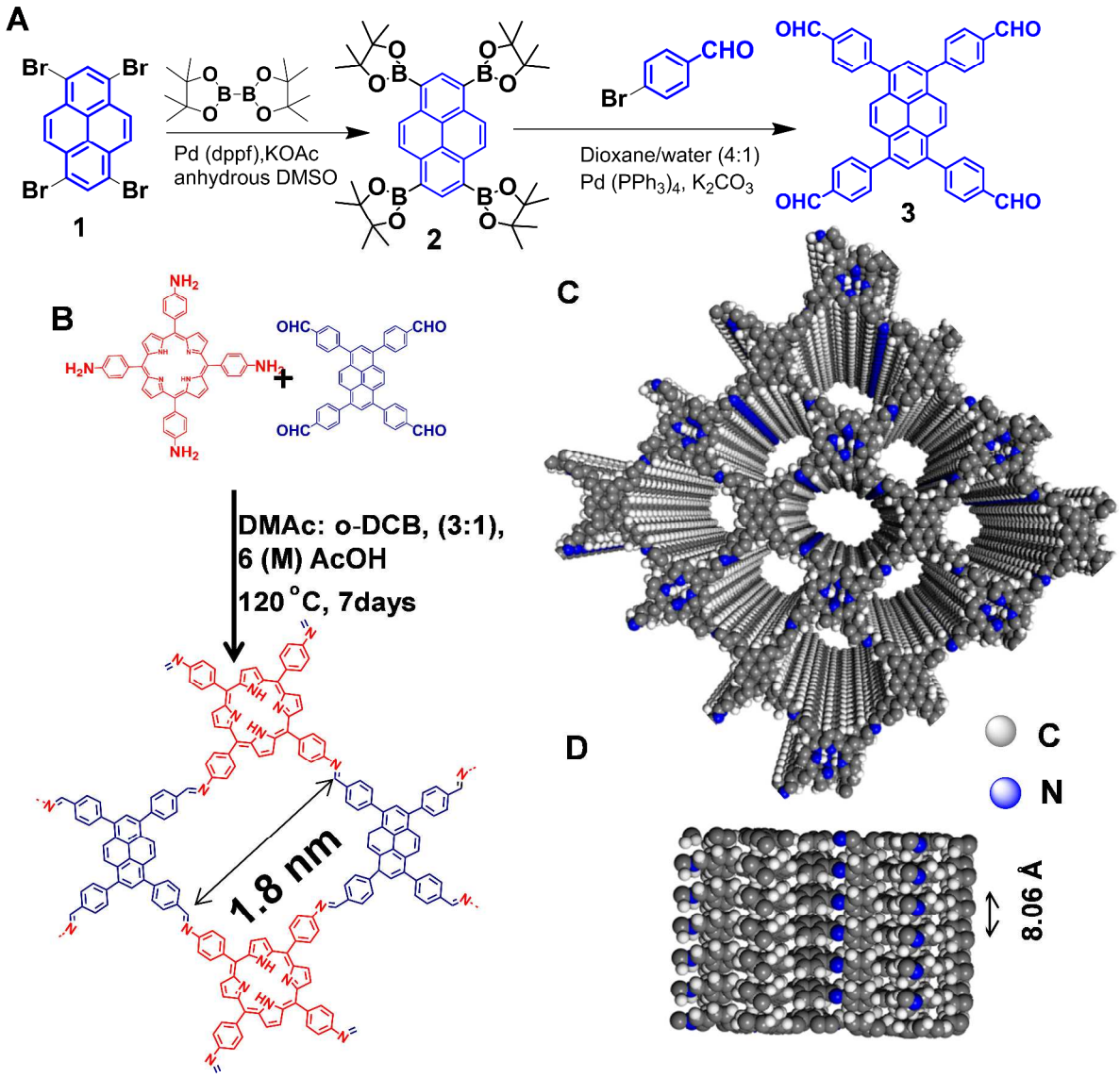

Figure 1. (A) Synthesis of 1,3,6,8-tetrakis(4-formylphenyl) pyrene (TFFPy) (B) Synthetic scheme of the imine based COF (SB-PORPy). (C) Top view (D) Side view of AA (eclipsed) stacking of SB-PORPy COF (gray: carbon, blue: nitrogen)

Figure. 2

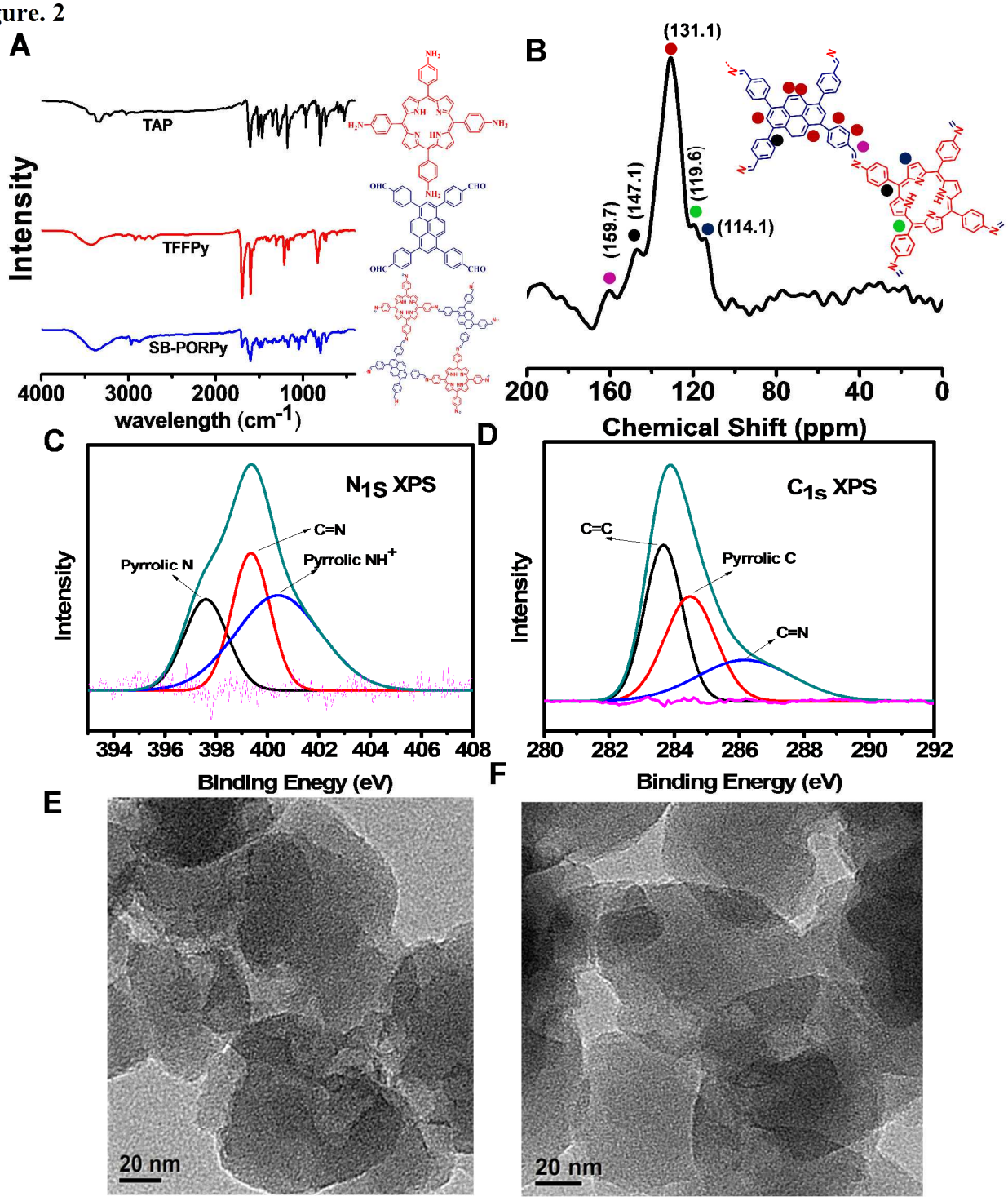

Figure 2. (A) IR spectra of SB-PORPy COF. (B) 13C solid state CP-MAS NMR of SB-PORPy-COF; (C) N1s peak SB-PORPy-COF and (D) C1s XPS peak. High resolution transmission electron microscopy of SB-PORPy-COF at different region (E, F).

Figure. 3

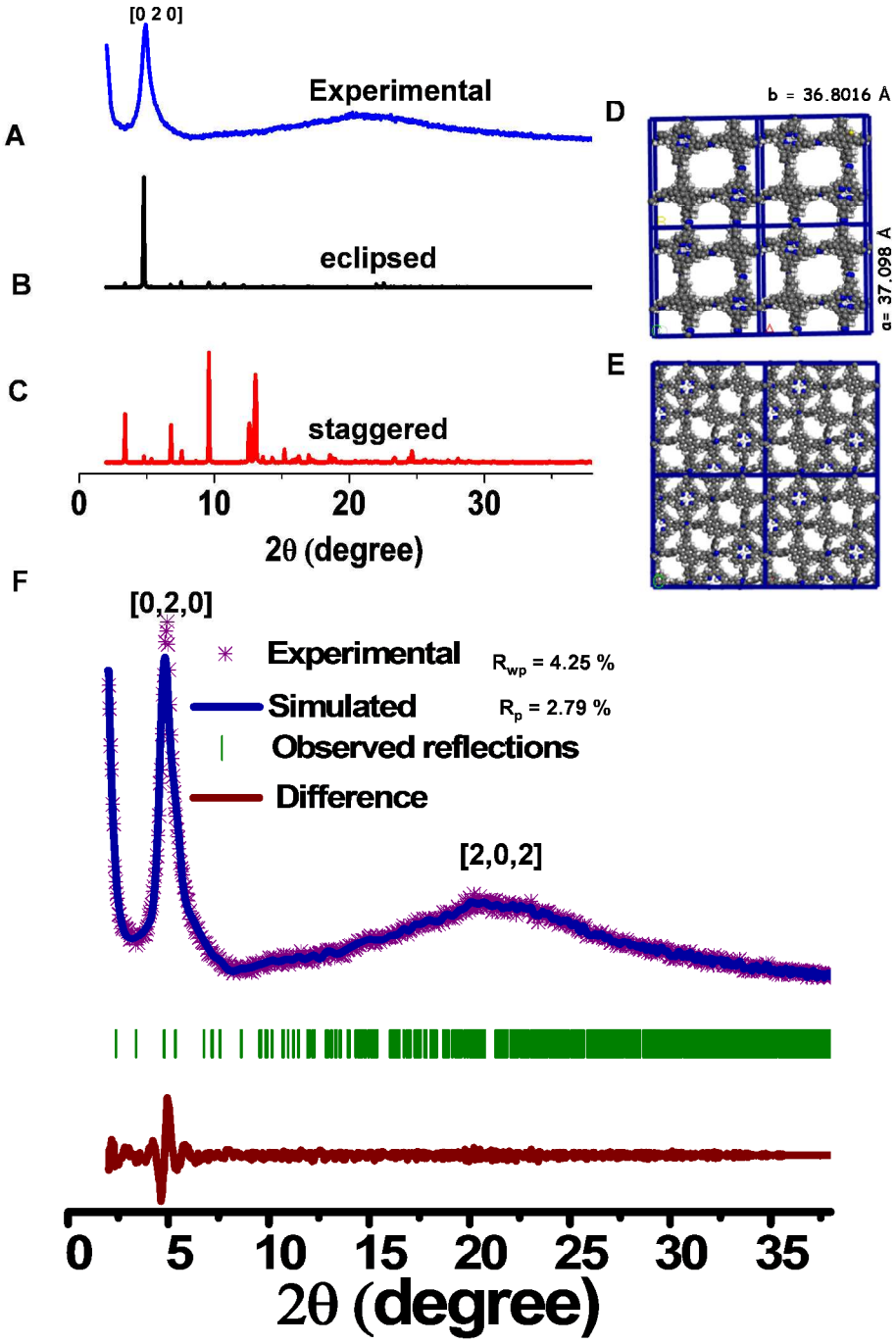

Figure 3. (A) Experimental PXRD (blue), (B) Theoretical AA (eclipsed) stacking (black), (C) Theoretical AB (staggered) stacking (red); (D) top view of simulated AA stacking and AB stacking (E) and Pawley refinement of PXRD (F).

Figure. 4

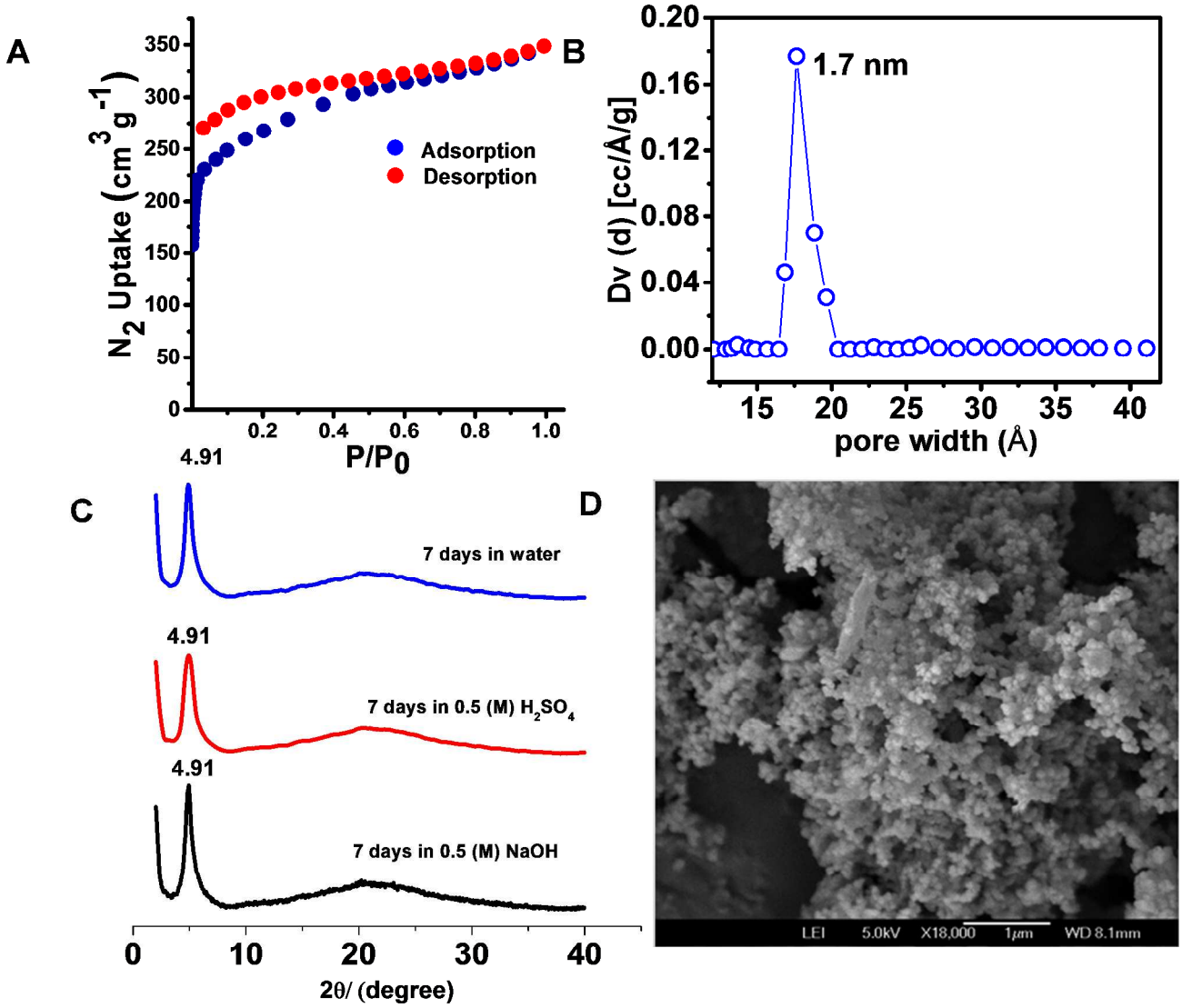

Figure 4. (A) N_2 adsorption (blue solid circle) /desorption (red solid circle) isotherm at 77K. (B) pore size distribution (blue empty circle). (C) Stability of SB-PORPy-COF in aquous, acedic and alkaline media. (D) SEM image of SB-PORPy-COF

Figure. 5

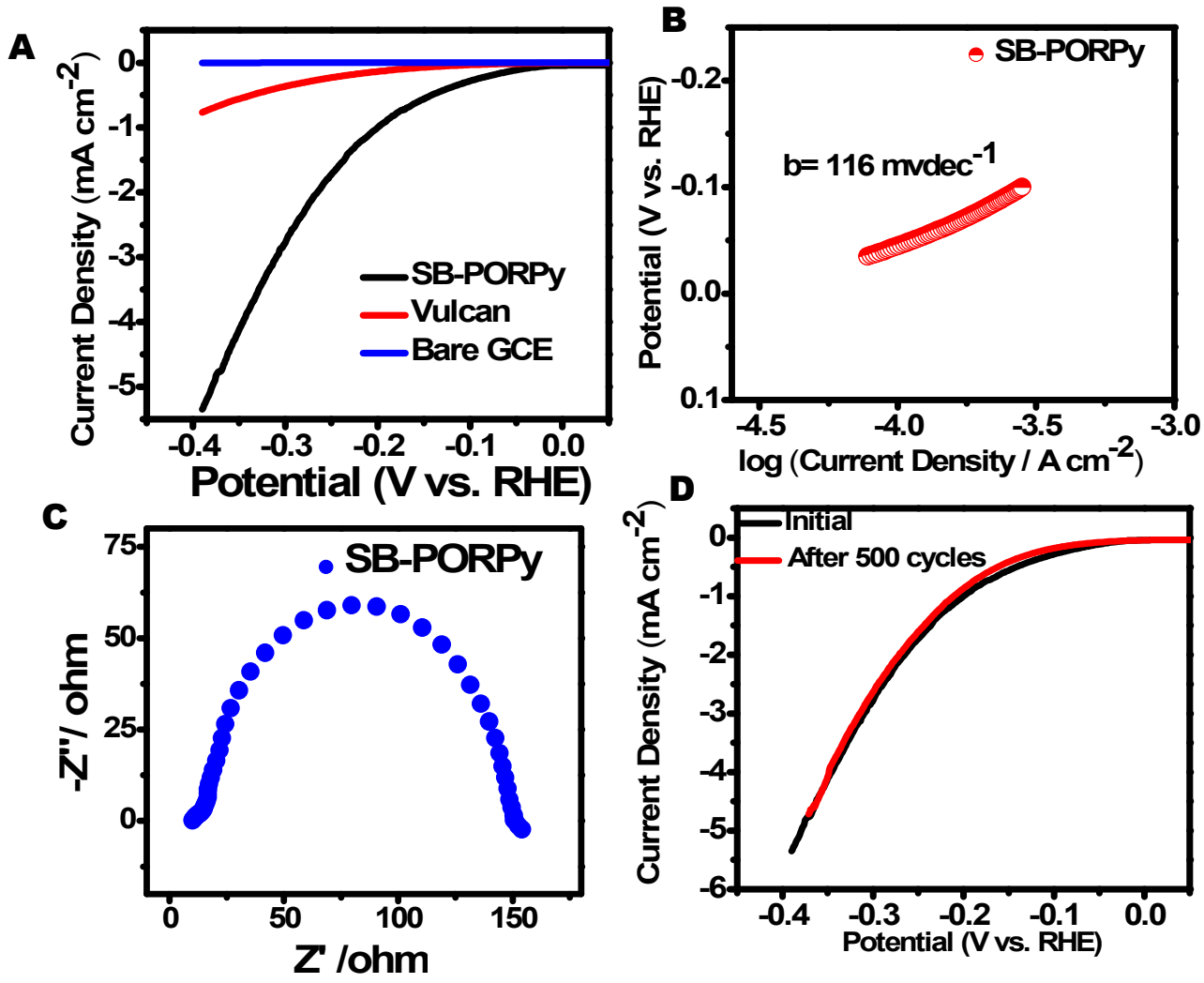

Figure 5. (A) Polarization curves for the hydrogen evolution reaction on bare GC (blue), Vulcan (red) and SB-PORPy-COF (black) electrodes. (B) Corresponding Tafel plot of SB-PORPy-COF electrode. (C) Impedance spectra (Nyquist Plot) of SB-PORPy-COF catalyst. (D) Linear sweep voltammograms of SB-PORPy-COF catalysts.

Figure. 6

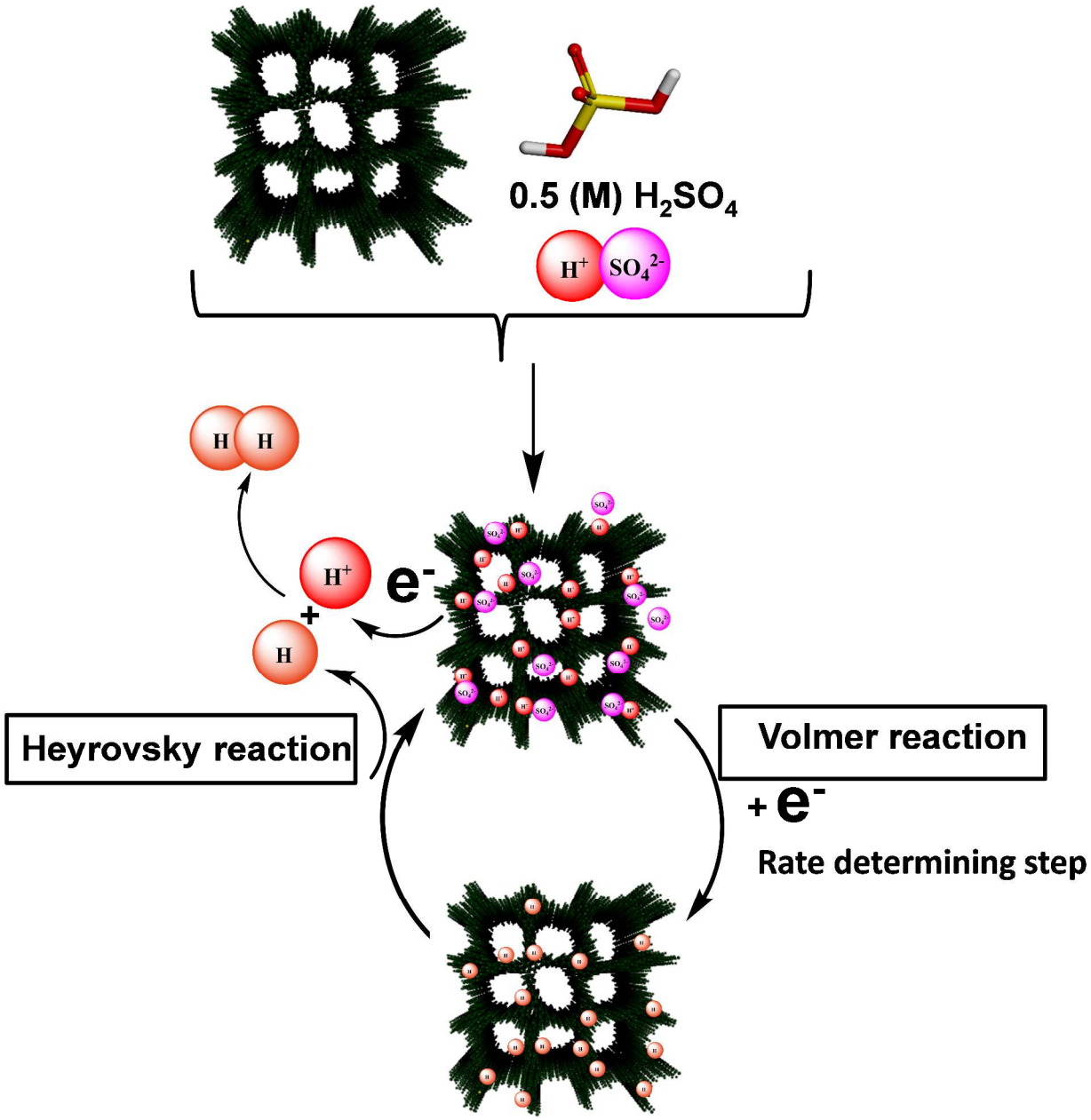

Figure 6. Possible volmar-heyrovsky pathaway of hydrogen evolution reaction on SB-PORPy-COF

Electrochemical Stimuli Driven Facile Metal Free Hydrogen Evolution from Pyrene-Porphyrin Based Crystalline Covalent Organic Framework.

Subhajit Bhunia,[†,‖] *Sabuj Kanti Das,*[‡,‖] *Rajkumar Jana,*[§] *Sebastian C Peter,*[§] *Santanu Bhattacharya,*[*,†] *Matthew Addicoat,*[*,¥] *Asim Bhaumik ,*[*,‡] *and Anirban Pradhan*[*,†]